Indoor Localization Strategy Based on Fault-tolerant Area Division for Shipboard Surveillance

Kezhong Liu[a,b], Mozi Chen[a,*], E Cai[a], Jie Ma[a,b], Shoujun Liu[c]

[a]*School of Navigation, Wuhan University of Technology, Wuhan, China*
[b]*Hubei Key Laboratory of Inland Shipping Technology, Wuhan, China*
[c]*School of Information Engineering, Wuhan University of Technology, Wuhan, China*

Abstract

Localization based on wireless sensor networks has been shown to be a promising application in ships. Although a considerable number of algorithms have been designed for low-overhead and high-accuracy localization, some problems have been ignored, such as interference in the shipboard environment and the method of using anchor-deploying. In this paper, we present a method for range-free localization called fault-tolerant area division (FAD) to deploy and divide the area in which precise indoor localization is required. Despite the limitations with respect to shipboard environmental interference, sensing irregularity, received signal strength variation, and other unavoidable factors, FAD has been shown to be reliable by improving the fault-tolerant mechanism. In addition, to address the scheme of anchor-node placement, which complicates the localization performance, this paper presents a new deployment strategy for the anchor nodes using optimization methods. This paper presents and analyzes an enhancement method using a series of simulations and real-world ship experiments. The result shows that a well-organized deployment and a fault-tolerant mechanism can make such localization method more reliable and compatible.

Keywords: Indoor localization, Shipboard Location Discovery, Area division, Signal strength

*Corresponding author
Email address: chenmz@whut.edu.cn (Mozi Chen)

1. Introduction

As cruise vessels and passenger ships are widely used for commercial purposes such as transporting passengers and cargo, there has been an increasing demand for automation techniques in ships that improve the ships operation and intelligent monitoring[1]. There have been several previous cases that have highlighted how complex and chaotic the movement of people on a large vessel can be during emergency situations. An accurate and pervasive shipboard indoor localization system for crew members and passengers would enable a rapid response to emergency incidents, and dramatically reduce the time needed to bring the ship under control[2]. Currently, the global positioning system (GPS) is the most effective positioning technology in outdoor environments. However, it has some weaknesses, such as being easily blocked by steel and poor signal strength in the shipboard indoor environment[3]. These have led to the development of indoor localization techniques such as radio-frequency ID (RFID), ultrawideband (UWB), and received signal strength indication (RSSI)[4] [5]. Among these technologies, wireless sensor networks (WSNs), which have been universally motivated by area surveillance applications, have been considered for deployment in the shipboard environment, and have been used for applications to localize objects and ensure the safety[6]. In addition, there is an increasing demand for low-cost and high-accuracy solutions as several WSN-based localization methods have emerged over the years.

In general, WSN-based localization mechanisms fall into two categories: range-free[7] [8], and range-based[9]. The range-based methods mainly utilize the RSSI to estimate the range from wireless base stations (called anchors) in order to calculate the location of target nodes (or unknown nodes). To obtain the precise range information, complex models for signal propagation[10][11], specialized time-synchronization hardware[4] [12] [13], and dedicated analysis for non-line of sight (NLOS) signal propagation[14] are required. While range-based methods require expensive hardware and high computation cost, range-free methods, which require less range information, are more suitable for large-scale sensor networks[15]. The range-free method has been studied in many algorithms, such as fingerprint techniques[16] [17], wireless connectivity [18] [19] [20], anchor proximity[11], and landmarks[21] [22]. Among them, fingerprint-based techniques focus on the radio statistic features of the localization space, and they require the extensive exploitation of existing infrastructures[23]. Wireless connectivity methods, such as DV-Hop[19], use

local sensing to estimate the virtual distances of the anchors in large-scale sensor network localization. Wireless local area network (LAN) controllers (WLCs)[11] use RSSI as the weight to calculate the centroid of neighbor anchors, and to achieve high accuracy. In fact, most of these methods can be severely affected by the dynamic shipboard environment. The localization accuracy can be significantly degraded owing to the poor signal strength as a result of shielding by the steel framework of ships. In addition, they do not consider that the deployment of anchor nodes is important to the robustness of range-free localization schemes used in narrow enclosed spaces.

The phenomenon in shipboard environments is clearly different from the traditional indoor environment. In a real shipboard environment, the decks and walls are steel frames that generate different multipath effects and lead to severe reflection of wireless signals[24] [25]. Meanwhile, signal propagation suffers from dynamic changes during a given voyage, including transient interferences, such as moving subjects, opening and closing doors, and prolonged changes in terms of the ship speed, temperature, humidity, and weather conditions. Therefore, the RSSI in the shipboard is considered to be a complex combination of many factors, such as radio path-loss factors, metal reflection, multi-path effects, and ship engine noise[10] [26], and it is complicated to use it to obtain localization signatures. Unfortunately, most of the proposed localization methods are based on the general assumption that the environment is interference-scarce . These algorithms cannot achieve high performance where RSSI signals are so unreliable, and they are prone to be disturbed in the shipboard environments. Our work is motivated by the observation that the localization signal may suffer from the severe RF fading problem in shipboard environments, and deals with this problem effectively by using the high–low relationship of RSSI and a fault-tolerant mechanism.

In this paper, we first study the shipboard environment and propose a new lightweight localization method that is called fault-tolerant area division (FAD), based on the high–low relationship of RSSI. First, we study the relationship between RSSI and the physical distance in shipboard scenarios based on applying the model-fitting technique, and we observe that the fallibility and fuzzy boundaries problem existed. Second, FAD focuses on the high–low relationship instead of the absolute value of the RSSI, and divides the whole shipboard environment into several subareas that are marked by different unique RSSI-distance relations. To take advantage of the area-division model, a fault-tolerant mechanism is presented to achieve a fine-grid localization result that makes the algorithm less likely to be affected by the RF-fading

and boundary-fuzziness problems. Third, to enhance the performance of FAD in the shipboard environment, we optimize the anchor placements and avoid the problem of vicious subareas. The heterogeneity of subareas, which can be theoretically analyzed by the subarea standard deviation and convergence level, can improve the localization accuracy significantly. Finally, the simulation and experiment results indicate that FAD provides a better accuracy than the other four state-of-the-art range-free localization techniques over a range of node-deployment conditions. The proposed method improves the range-free localization accuracy based on RSSI with reduced workload, and it can be applied to shipboard indoor localization applications appropriately. The main contributions of this study are as follows: The main contributions are as follows:

1. Localization based on WSNs may suffer from severe disturbances in the shipboard environment, where the RSSI is affected by the steel structure and dynamics of the shipboard environment. We propose FAD based on the high–low relationship between RSSI pairs instead of absolute RSSI values, which is less affected by the RF interference.
2. According to the structure of real-world ships, FAD divides the whole shipboard space into several subareas that are marked by different unique RSSI relations. In addition, a fault-tolerant mechanism is proposed to take advantage of the fallible localization subarea, and more accurate localization results can be achieved.
3. To enhance the robustness of FAD, we propose an anchor deployment strategy that utilizes the optimization method to achieve a minimum standard deviation of all subareas as well as to maintain the maximum number of subareas.

The rest of the paper is organized as follows. Section 2 briefly describes the theoretic basis of the FAD. Section 3 explores the main challenges that are associated with shipboard localization methods. In Section 4, details of the solutions and the system design are presented. Sections 5 and 6 evaluate the method with extensive simulations, and make several comparisons with the state-of-the-art localization algorithm. Section 7 presents the related works, and Section 8 concludes the paper.

2. Theoretic Basis of FAD

This section briefly describes two ideas: the propagation model of wireless signals in the shipboard environment and the area-division model, which are the basis of the FAD. First, we conducted several experiments in a ship and found that the relative RSSI from anchor nodes can be utilized to mark different area locations, as opposed to the actual values. Then, we introduce the concept of the area-division model, which utilizes the high–low relationship of RSSIs and the perpendicular bisectors of anchor locations to divide the area into several subareas that own unique marks. Our discussion starts with a two-dimensional (2D) paradigm to describe how the area-division model is used to localize the targets.

2.1. Preliminary Experiments

The RSSI distribution models have been well studied in [10]. According to the radio propagation model, the path loss in a general location is random and has a log-normal distribution about the average distance value. The average commonly used path-loss model is expressed as a function of the distance as

$$PL(d) = PL(d_0) + 10n \log(\frac{d}{d_0}) + X_\sigma \tag{1}$$

where $PL(d)$ represents the path loss. n is the path-loss exponent, which indicates the rate at which the path loss increases with distance, d is the signal receiving distance, and $d_0 = 1$m is a reference distance. X_σ is a zero-mean Gaussian distributed random variable (in dBm) with standard deviation σ.

We performed several experiments to estimate the average losses in a passenger ship called "M.S.Yangtze 2," as shown in Fig. 1. Experiments were carried out in several typical shipboard scenarios, such as on the sun deck, a dining hall, a corridor, and an emergency gangway. Fig. 3 shows the measurement data and corresponding distance for the path losses in the above environments. A nonlinear regression with the target function of a minimum mean-square error is utilized to determine the path-loss parameters of each shipboard environment. The path-loss parameters are shown in Table 1.

As can be seen, shipboard scenarios share different signal propagation parameters. The range-based methods, which utilize RSSI to estimate the range from anchors, are not workable in the shipboard environments. Instead, a relationship model, where the RSSI is inversely proportional to the distance,

Figure 1: The Experiment passenger ship M.S.Yangtze 2.

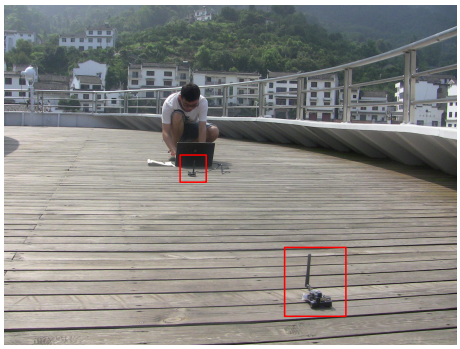

(a) Sun deck

(b) Central hall

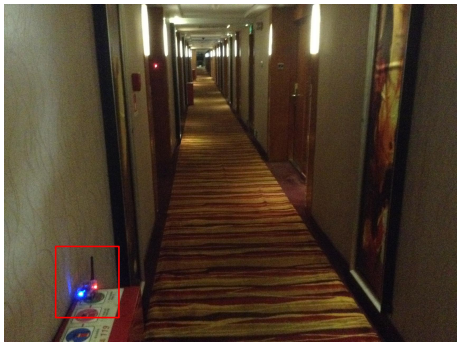

(c) Corridor

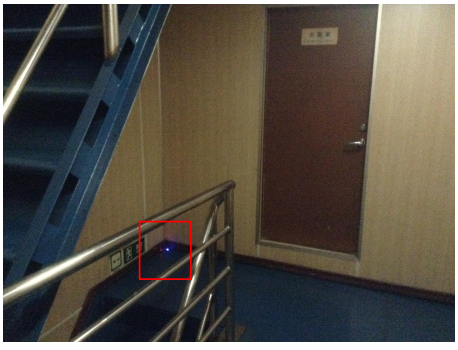

(d) Emergency gangway

Figure 2: Different experiment scenarios in M.S.Yangtze 2.

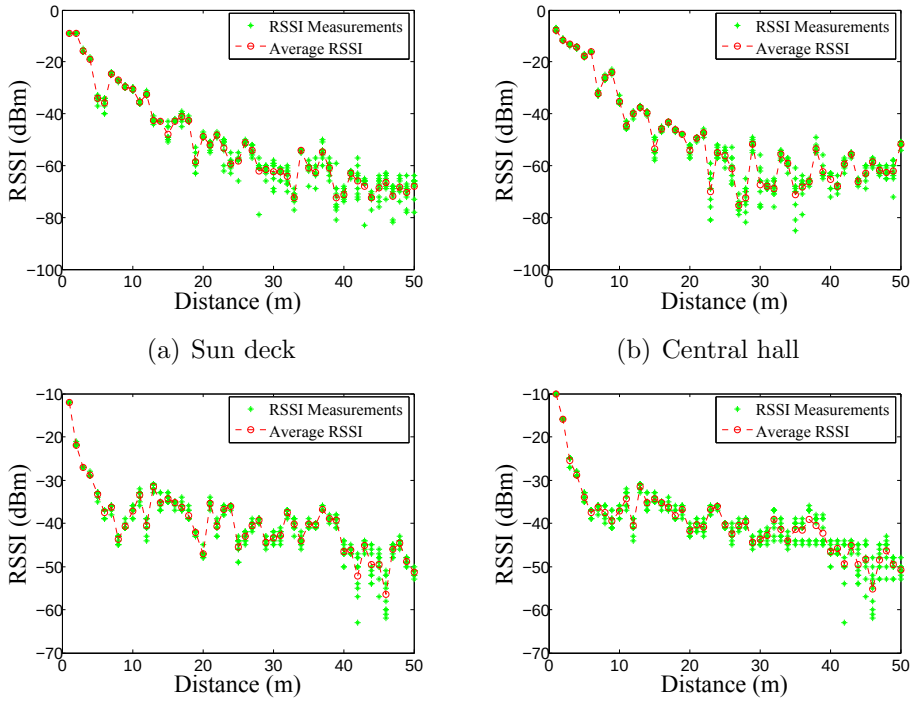

(a) Sun deck (b) Central hall

(c) Corridor (d) Emergency gangway

Figure 3: RSSI Measurements with different distances.

Table 1: Path loss parameters in different shipboard scenarios.

Scenarios	**n**	σ	γ	$PL(d_0)$
Corridor	-1.7	8.06	0.80	-7.7
Central hall	-1.4	7.13	0.83	-9
Dining hall	-0.9	5.16	0.66	-8
Passenger cabin	-0.8	4.67	0.62	-8.9

is shown in our results. The high–low relationship of RSSI can be more reliable than the actual values to indicate the location signature. We can use this property to mark locations and realize the location discovery.

2.2. Area Division model

In this section, we define the area-division model and illustrate them using examples. As shown in Fig. 4, the proposed model consists of two critical components: the map division and the RSSI signatures used in localization. The area-division model divides the localization space into several subareas based on the location of anchors, and the space is marked with corresponding RSSI high–low relations. By measuring the RSSIs from available anchors, the physical information can be converted into RSSI signatures, and we can determine the subarea to which the unknown node belongs. To illustrate our concept, we start from a basic scenario in which there are no barriers between any anchor pairs. Taking an area with two anchors, P_1 and P_2, as shown in Fig. 4(a), the vertical bisector of P_1 and P_2 divides the localization space into two subareas, and their relative distances will be computed. Each position on the left side of the bisector will be closer to anchor P_1, which implies that the RSSI from anchor P_1 will be stronger than that from anchor P_2. Using perpendicular bisectors, an area can be divided into several subareas. Each subarea owns a unique high-dimensional location signature consisting of an RSSI high–low relationship. Once a target gets into the area, the location can be computed by comparing the RSSI from each anchor, and determine the subarea which it belongs. Our discussion starts within the context of a 2D paradigm, although the algorithm also applies to a three-dimensional (3D) paradigm. Cases that involve three or more anchor nodes are shown to be similar.

Definition 1. *A **Boundary** is a vertical bisector of two anchor positions.*

Definition 2. *A **Subarea** is an area that is segmented by boundaries.*

As the example shows in Fig. 4(a), the boundary $L_{1,2}$ divides the localization space into two distinct subareas. The target node Q_1 measures the RSSI from both anchors (P_1 and P_2), and obtains $RSSI_{P1} > RSSI_{P2}$. According to the propagation model in Section 2.1, the location of Q_1 is close to the anchor node P_1. Therefore, Q_1 belongs to the shadow subarea. Similarly, Fig. 4(b) shows that three anchors (P_1, P_2, and P_3) generate three boundaries ($L_{1,2}$, $L_{1,3}$, and $L_{2,3}$) and six subareas. Q_2 obtains $RSSI_{P1} > RSSI_{P2}$,

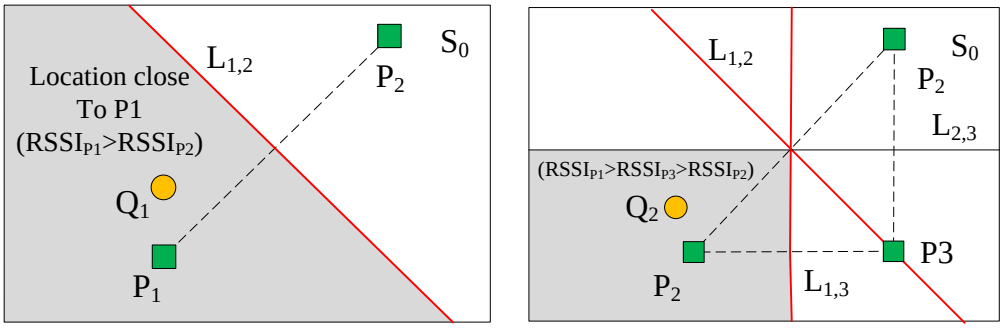

(a) Two anchors (b) Three anchors

Figure 4: Description of the area-division model.

$RSSI_{P1} > RSSI_{P3}$, and $RSSI_{P2} < RSSI_{P3}$. Therefore, Q_2 belongs to the subarea marked in the figure. Ultimately, the centroid of the subarea is the estimated location. Based on the above examples, we can conclude that increasing the number of anchor nodes can divide the original space into more subareas, which can provide a fine-grid location information of the target nodes.

3. Design Challenges

Although the area-division method avoids most problems that occur in range-free methods, three main challenges for the proposed method are as follows.

3.1. Fallibility Boundary

Definition 3. ***Fallibility Boundaries*** *are two lines parallel to the boundary with a distance of* ΔD.

According to the experiment results shown in Section 2.1, the RSSI received from two anchors would be similar when the target node is close to the boundary. Further, the dynamic ship environment would introduce noise into the RSSI measurement. The target nodes, which lie in the fallibility boundaries, would receive a converse high–low relationship of the RSSI and wrongly determine their own subarea. As illustrated in Fig. 5, a boundary L is drawn based on two anchor nodes P_1 and P_2, which divides the plane into two subareas. A target node Q_1 lies near to the boundary. The target

node obtains the $RSSI_{P1}$ from P_1, and $RSSI_{P2}$ from P_2. Owing to the fluctuation in the RSSI values, we may obtain $RSSI_{P1} < RSSI_{P2}$, which would incorrectly determine that node Q_1 is in the wrong subarea. The fallibility boundaries are the dotted lines that bound the fallible localization subarea.

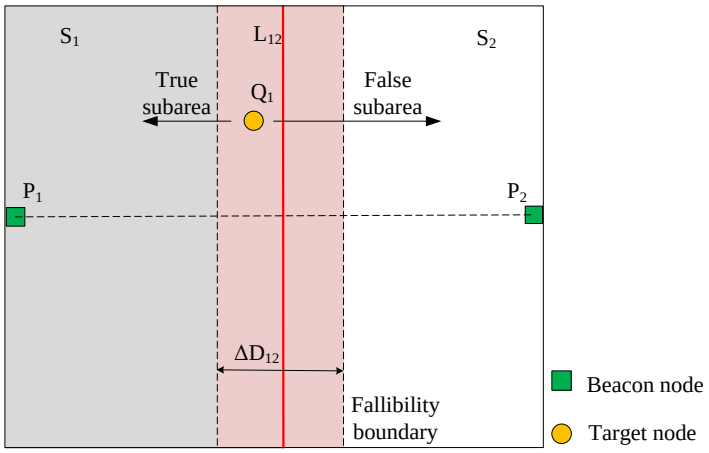

Figure 5: Description of fallibility boundary.

3.2. RSSI Deteriorate

Definition 4. *A **fuzzy boundary** is an arc for which the center is the anchor node and the radius is the reliable range.*

The reliability of RSSI signals will deteriorate rapidly when the distance exceeds the reliable range. As can be seen in Fig. 3(b), the RSSI value continues to decrease as the distance increases when the distance is less than 25 m. After that, the RSSI values fluctuate at around -60 dBm. This critical distance is called the reliable range. When the communication distance exceeds the reliable range, the variance of RSSI will increase and the high–low relationship of RSSI will become unreliable. The concept of the fuzzy boundary is illustrated in Fig. 6. The anchor nodes P_1 and P_2 are deployed on both sides of the localization space. For the target node Q_1, which lies outside of the fuzzy boundaries of anchors, it is difficult to determine the subarea to which it belongs. Hence, there is the need for a fault-tolerant design of the area-division model for shipboard environments. We solve this challenge by combining the limited prior information and current sensing data to provide a balanced area division.

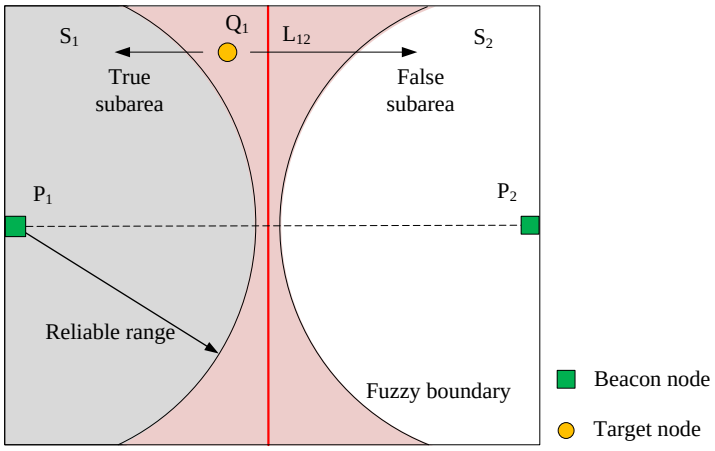

Figure 6: Description of fuzzy boundary.

3.3. Anchor Node Deployment

Different anchor-deployment strategies would generate different sets of subareas. The placement of anchors impinges on the number of subareas, and a greater number of subareas means that there are more precise locations. As illustrated in Fig. 7, with the same number and density of anchor nodes, the number and distribution of the subarea vary. We deployed three anchor nodes in a rectangular space. Fig. 7(a) shows that there are four subareas, each having an identical shape. In contrast, Fig. 7(b) shows that we can obtain two more subareas, and Fig. 7(d) shows that we can obtain uniform shapes of six subareas by adjusting the positions of the anchors. After the simulation, the result shows that the scheme (a) achieves the worst localization effect, while that in (b) achieves the best. Therefore, this provides the motivation for us to search for the optimal anchor deployments. An efficient method of improving the localization accuracy is to deploy the anchors in a particular manner, where the number of subareas is as large as possible, and where they have a uniform shape. To simplify the problem, we choose the standard deviation of division subareas as a metric in our algorithm. Then, we adopt similar traversing techniques as we did in the previous section to conduct experiments.

4. Proposed Method

In this section, we discuss specific solutions for the challenges mentioned in Section 3. We propose a fault-tolerant mechanism of the fallibility/fuzzy

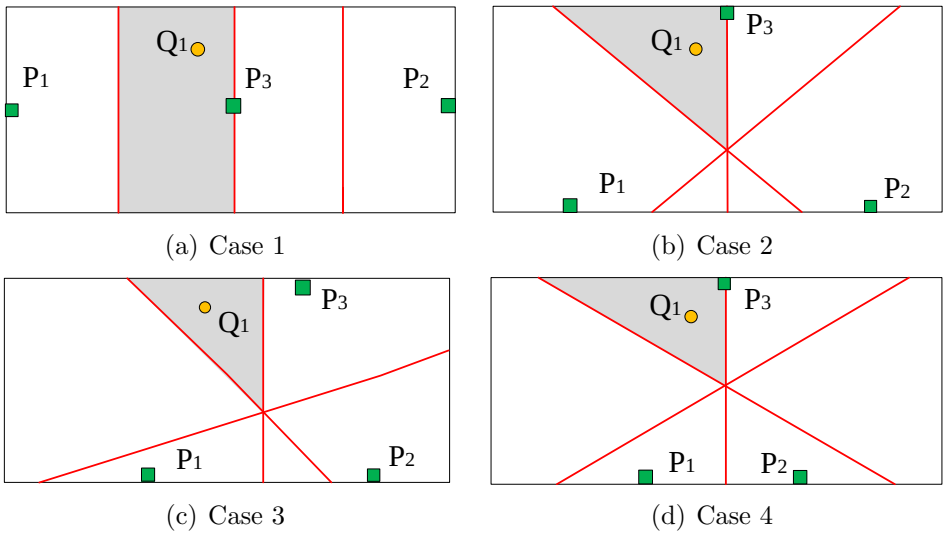

(a) Case 1 (b) Case 2

(c) Case 3 (d) Case 4

Figure 7: Different anchor deployments.

boundaries, which generates fine-grid subareas and reduces the positioning error. We also discuss the optimal anchor-deployment strategy.

4.1. Fault-tolerant Model Adjustment

Definition 5. *A **correcting subarea** is an area that is segmented by fallibility boundaries and fuzzy boundaries.*

A. Fallibility Boundary Mechanism

With the basic theory of the FAD, the position information of an area can be abstracted to a high–low relationship of RSSI from anchors that have been deployed. However, the fallibility boundary problem may lead to an erroneous relationship and an incorrectly estimated subarea. To solve this problem, we propose a fault-tolerant scheme of the fallibility boundary. Fallibility boundaries are two lines that are parallel to the boundary with a distance of ΔD. The subarea, which is separated by the fallibility boundary, is identified as a correcting subarea. As shown in Fig. 8, two boundaries are accompanied by four fallibility boundaries. The 2D space can be divided into four subareas and five correcting subareas. In the fallibility boundary mechanism, when there is a large difference between the RSSI values measured from anchors, the target node location would be the centroid of the subarea generated by the two anchor node boundaries. Conversely, when the

RSSI values are similar, the target node location would be the centroid of the correcting subarea.

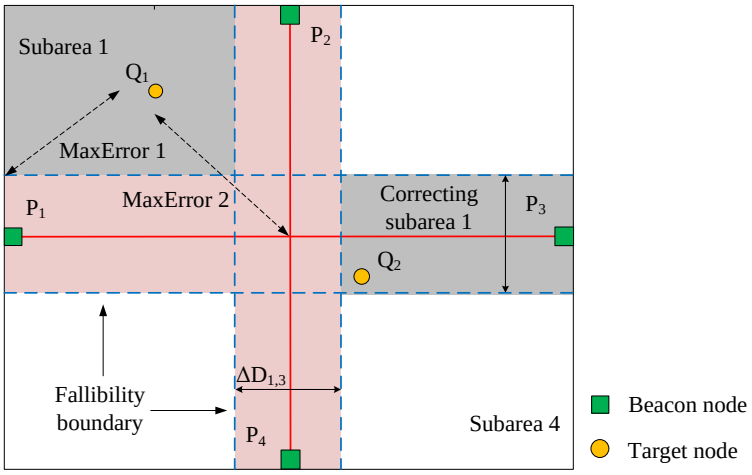

Figure 8: Fallibility boundary mechanism

In Fig. 8, the target node Q_1 obtains the RSSI information for $|RSSI_1| > |RSSI_3|$ and $|RSSI_2| > |RSSI_4|$. According to the area-division model, the position of Q_1 should be close to P_1 and P_2. Meanwhile, the absolute values of the differences in the RSSI can be calculated as follows: $|RSSI_1 - RSSI_3| > \Delta RSSI_{1,3}$ and $|RSSI_2 - RSSI_4| > \Delta RSSI_{2,4}$. Therefore, the position of Q_1 is outside of the fallibility boundary of $L_{1,3}$ and $L_{2,4}$, and it belongs to subarea 1 shown in shadow area. Similarly, the target node Q_2 obtains the information that $|RSSI_3| > |RSSI_1|$, $|RSSI_4| > |RSSI_2|$, $|RSSI_1 - RSSI_3| < \Delta RSSI_{1,3}$, and $|RSSI_2 - RSSI_4| > \Delta RSSI_{2,4}$. According to the model, the position of Q_2 is close to P_3 and P_4, and it lies in the fallibility boundary of $L_{2,4}$ and outside of the fallibility boundary of $L_{1,3}$. The location of Q_2 belongs to the correcting subarea 1 shown in the shadow area.

The distance ΔD is correlated to the distance between the two anchors, and it is 10%–15% of the distance between anchors P_1 and P_2. The $\Delta RSSI$ values are shown in Table 2. The fallibility boundary mechanism provides useful location information for higher accuracy localization.

Proof for Fallibility Boundary Mechanism:

(1) To As seen in the Fig. 8, we find that:

$$S_1 = (d_{1,3}/2) \times (d_{2,4}/2)$$

Table 2: Relation between the distance of beacon nodes and ΔD.

$d_{P1,P2}$(m)	1	5	10	20	30
$\Delta D_{1,2}$(m)	0.1	0.5	1.2	3	4.5
$\Delta RSSI_{1,2}$(dBm)	2	2	2	3	5

$$S_2 = (d_{1,3}/2 - \Delta D_{1,3}/2) \times (d_{2,4}/2 - \Delta D_{2,4}/2)$$

where d_{13} represents the distance between nodes P_1 and P_3, and d_{24} represents the distance between nodes P_2 and P_4. S_1 represents the area of the primal subarea 1 whose boundaries are $L_{1,3}$ and $L_{2,4}$. S_2 represents the area of the new subarea 1 whose boundaries are fallibility boundaries. Therefore, we find that $S_1 > S_2$, and the fallibility boundary mechanism can achieve a fine-grid localization result.

(2) Denote the maximum location error of S_1 as $MaxError1$. It can be obtained by calculating the distance from the centroid of the subarea to its furthest vertex. $MaxError2$ represents the maximum location error of S_2. We obtain:

$$MaxError_1 = \sqrt{(d_{24}/4)^2 + (d_{13}/4)^2}$$

$$MaxError_2 = \sqrt{(\Delta D_{13})^2 + (d_{24}/2 - \Delta D_{24})^2}$$

It is clear that $MaxError_1 > MaxError_2$. This proves that the fallibility boundary mechanism can provide fine-grid subareas and higher accuracy.

B. Fuzzy Boundary Mechanism

In this section, we discuss another key technique in FAD, namely the fuzzy boundary mechanism. We introduce the area-division problem based on an ideal RSSI distribution assumption. However, the disaffinity distribution of RSSI from different devices shown in Fig. 3 will cause an inaccurate location estimation problem when it comes to a practical application.

For further discussion, we define the following concept: After anchors with different RSSI peaks are deployed, the division boundaries will become arcs rather than straight lines. To solve the deterioration problem associated with RSSI stability, we proposed a fault-tolerant fuzzy-boundary scheme. Fuzzy boundaries are arcs that are drawn by the reliable ranges of each anchor. The subareas are divided by fuzzy boundaries, and new correcting subareas are generated accordingly. When the RSSI values measured from anchors exceed the reliable range, the target node location would be the centroid of the correcting subarea generated by the anchor fuzzy boundaries. By utilizing the fuzzy boundaries and fallibility boundaries, we can obtain more precise and more accurate results of localization in the shipboard environment.

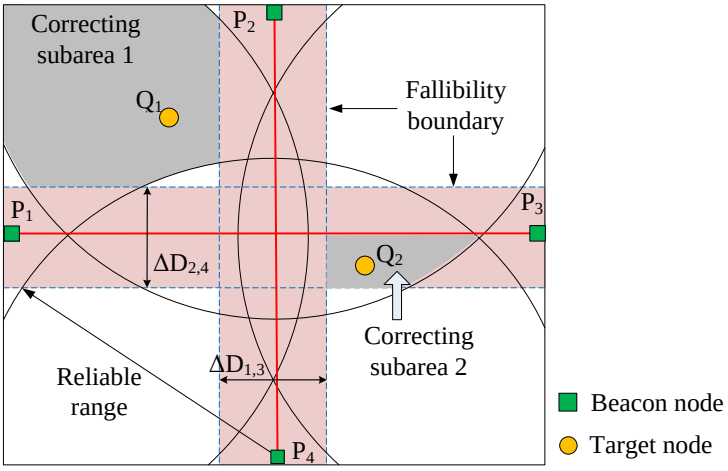

Figure 9: Fuzzy boundary mechanism.

As illustrated in Fig. 9, the target node Q_1 obtains the RSSI information as $RSSI_1 > RSSI_3$ and $RSSI_2 > RSSI_4$. The absolute values of their difference are $|RSSI_1 - RSSI_3| > \Delta RSSI_{1,3}$ and $|RSSI_2 - RSSI_4| > \Delta RSSI_{2,4}$. Therefore, the position of Q_1 is outside of the fallibility boundaries of $L_{1,3}$ and $L_{2,4}$. Meanwhile, we can show that $|RSSI_1| < Threshold$, $|RSSI_2| < Threshold$, $|RSSI_3| > Threshold$, and $|RSSI_4| > Threshold$. Then, the target node Q_1 should be within the fuzzy boundary of P_1 and P_2, and outside of the fuzzy boundary of P_3 and P_4. Therefore, the position of Q_1 should belong to the correcting subarea 1 shown in the shadow area. Similarly, the position of target node Q_2 is within the fuzzy boundary of P_2, P_3, and P_4, and outside of the fuzzy boundary of P_1. Meanwhile, Q_2 lies within the fallibility

boundary of $L_{1,3}$ and outside of the fallibility boundary of $L_{2,4}$. Therefore, the location of Q_2 can be determined in the correcting subarea 2, as shown in the figure.

Table 3: The reliable range in different shipboard scenes.

Scenarios	Corridor	Central hall	Dining hall	Engine room
Reliable range (m)	15	20	50	25
Threshold (dBm)	-54	-51	-49	-52

It can be seen that each subarea only owns one identification RSSI relationship. Therefore, we can generalize it to apply to more anchor scenes. Here, the reliable range of each node corresponds to the environment, and it can be determined based on the experiment analysis. We can calculate the threshold according to the model in Section 2.1. The shipboard reliable range and threshold are obtained as Table 3.

However, the fuzzy-boundary mechanism may lead to another problem called the vicious subarea, which affects the independence of the subareas. As shown in Fig. 8, the five vicious subareas, which are generated by four fuzzy boundaries, share the same relationship with the RSSI signals and scatter in different positions of the area. The location of the node Q_1 cannot be determined by the high–low relationship of RSSIs.

As demonstrated, the fuzzy boundaries may isolate one subarea into several vicious subareas, and this can be solved by a planned anchor deployment. This issue also contributes to our motivation to determine the optimal anchor deployments.

4.2. Anchor Deployment

The different anchor deployment can generate different numbers and shapes of subareas. With respect to deployment optimization, our goal is to eliminate the error rate and improve the accuracy of the FAD. We also seek to optimize its usage by avoiding the vicious division problem.

A. Subarea Amount

The first impact factor of the performance of FAD is the subarea amount (SA). Owing to the properties of the AD, it is possible to derive tighter

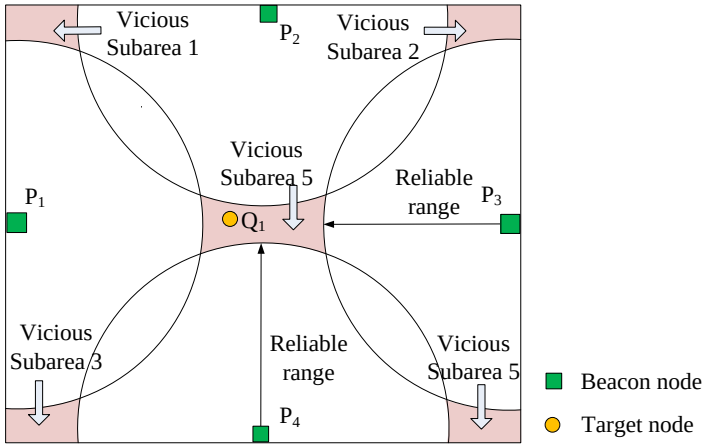

Figure 10: Vicious subarea.

upper bounds on the number of subareas. As discussed in Section 2.2, the number of subareas is equal to the sum of the number of areas created by the boundaries of anchor nodes. Therefore, we can obtain its upper bound by calculating the maximum number of boundaries. Assuming that there are n anchors in a 2D paradigm, the number of generated boundaries can be denoted as

$$boundries = \frac{n \times (n-1)}{2} \tag{2}$$

and the number of subareas can be denoted as:

$$SA = \frac{boundries^2 + boundries + 2}{2} \tag{3}$$

The maximum of SA can be denoted as:

$$SA_{max} = \frac{n^4 - 2n^3 + 3n^2 - 2n + 8}{2} \tag{4}$$

The steps taken to calculate the SA in FAD is as follows:

(1) To calculate the max SA of n anchors in a space, we calculate the max SA of $n-1$ anchors and add the increased subareas generated by the new boundary.
(2) When $n = 2$, the SA is two subareas. Therefore, the algorithm used to calculate the SA can be denoted as

$$\begin{cases} SA(N) = SA(N-1) + subArea(n, [n-1]), & n > 2 \\ SA(n) = 2, & n = 2 \end{cases}$$

where, $subarea(n, [n-1])$ denotes the addition subarea.

B. Subarea Convergence Level

The second impact factor is the subarea convergence level (SCL). The SCL is an indicator of the subarea convergence, and can be denoted as

$$SCL = \sum_{i=1}^{SA} (\frac{S_i}{S} \times MPC_i) \tag{5}$$

where SA represents the total number of subareas. S represents the area of the whole space, and S_i is the area of the i-th subarea. MPC_i represents the average length between the centroid and vertices of the i-th subarea.

C. Subarea Uniform Level

The third factor is the subarea uniform level (SUL). The SUL is an indicator of the subarea uniform, and can be denoted as

$$SUL = \sum_{i=1}^{SA} (\frac{S_i}{S} \times VPC_i) \tag{6}$$

where VPC_i represents the variance of the length between the centroid and vertices of the i-th subarea.

The anchor-deployment scheme in FAD will satisfy: Maximize SUL, Subject to $SA = SA_{max}$, and Minimize SCL. Note that in practice, deployment schemes can be evaluated by these three factors, and we can choose the better anchor placement in a particular area.

4.3. Localization Strategy

Below, the pseudocode of the proposed localization algorithm is presented.

The steps for the localization of target nodes using the fault-tolerant mechanism are given as follows:

Algorithm 1 Localization strategy

Require: The real coordinate of anchor nodes (X_i, Y_i), the number of anchor nodes n, the received signal strength of unknown nodes $RSSI(n)$, the RSSI constant of area misjudged ΔR and the effective precision range $Threshold$

Ensure: The unknown node estimate coordinate (x, y)

```
//For each anchor nodes
for i = 1 : n do
    make RSSI(n) into orderly vector
end for
select the 4th max members of RSSI(n) // Improve the efficiency of positioning
if RSSI(n) < Threshold then
    // satisfy the line area Division model
    if |RSSI(m) − RSSI(n)| < ΔR then
        perform the area division
    else
        perform the fallibility boundary mechanism
    end if
else
    perform the fuzzy boundary mechanism
    calculate the effective location area centroid
    output the unknown node estimate coordinate (x, y)
end if
```

(1) Draw the boundaries according to the positions of the anchor nodes and draw the fallibility/fuzzy boundaries based on the fault-tolerant mechanism. Determine all subareas and correcting subareas in the localization space.

(2) Measure the RSSI values between the target node and anchor nodes. Determine the high–low relationship of each RSSI, and compare them with the ΔRSSI.

(3) Determine the subarea of the target node using the area-division model. The centroid of the subarea is the estimated location of the target node.

5. System evaluation by Simulation

In this study, we performed a simulation performance evaluation of FAD. First, we present two criteria of the localization error, and then, by using simulations, we illustrate the performance of FAD and the anchor-node deployment strategy. We also present a comparative study with four other state-of-the-art localization methods.

5.1. Evaluation Criterion

In the localization procedure, each high–low relation of RSSI from anchor nodes maps to the centroid of the subarea that it represents. Representing all locations in a subarea by its centroid results in the cost of error in the location estimate result. Therefore, before the simulation, we present two criterions for the localization method. One is the mean error of the localization, which is shown as follows:

$$MeanError = \frac{1}{N} \times \sum_{i=1}^{N} (\sqrt{(X_i - x_i)^2 + (Y_i - y_{ij})^2}) \tag{7}$$

where N represents the number of target nodes. (X_i, Y_i) represents the estimated position coordinates, and (x_i, x_i) represents the actual position coordinates. The other is the error variance of the subareas, which is given as follows:

$$ErrorVariance = \sqrt{\frac{1}{N} \times \sum_{i=1}^{N} (E_i - MeanError)^2} \tag{8}$$

where E_i represents the localization error of the i-th target node. The lower the MeanError and ErrorVariance of the position, the higher will be the accuracy and reliability of the localization method.

5.2. FAD vs. AD

To illustrate the performance of the fault-tolerant mechanism, we compared the localization accuracy of the FAD and FAD without the fault-tolerant mechanism (called AD). We simulated 1000 unknown nodes and assumed that the node probability of the area misjudgment is 0.2, 0.4, 0.6, and 0.8. Then, we compared the mean localization error of the two algorithms in turn. As can be seen in Fig. 11, when the probability of the node

misjudgment gradually increases, the mean localization error and the localization variance calculated by AD also increase sharply; the result calculated by the localization method of FAD is relatively gentle, and the localization performance is best when $R = 5dBm$. We can see that the FAD provided an accuracy exceeding 30% compared to the AD. In ship environments, it is necessary to construct the localization fault-tolerant mechanism for unstable signals in ship cabins; otherwise, the accuracy and stability of the localization method of the AD will significantly decrease.

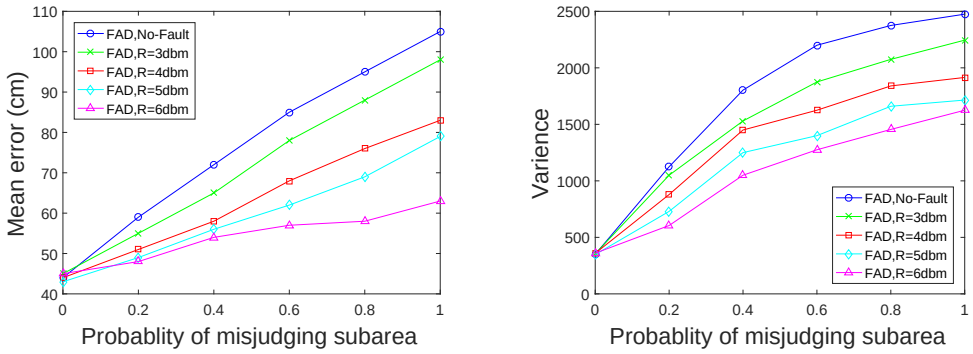

(a) Mean error (b) Varience

Figure 11: Performance of the fault-tolerant mechanism

5.3. FAD vs. four state-of-the-art Algorithm

In this section, we compared the localization result of the FAD method with WCL, REWL[11], SBL[27], and MGRD[28]. (Of them, SBL is an official implementation, and others are reproduced in this paper). The mean error and variance of the localization result are related. We performed multiple sets of comparative experiments that have the same experimental condition, hardware platform, and node-distribution density. Experimental results show that the FAD provides better accuracy and stability than the four other state-of-the-art algorithms. Fig. 12 shows a comparison of the mean localization error and standard deviation of the three algorithms. Table 4 shows the numeral position accuracy.

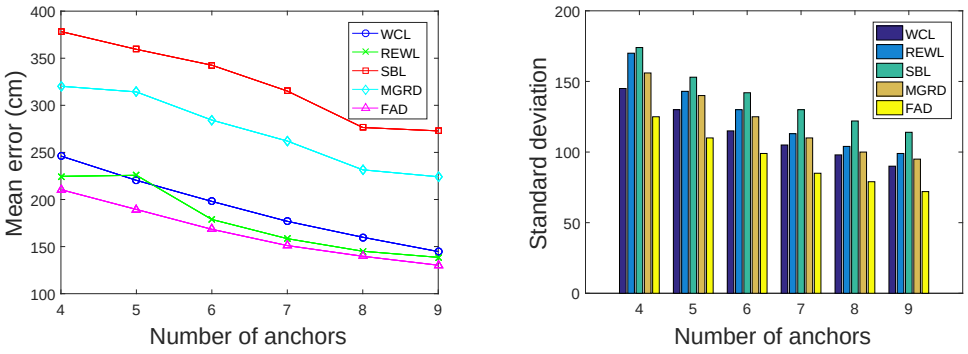

(a) Mean error (b) Standard deviation

Figure 12: Performance of three localization methods.

Table 4: Comparison of mean error (cm) in the simulation.

Methods \ Anchors	4	5	6	7	8	9
WCL	253.78	239.94	225.26	210.13	192.10	173.80
REWL	238.49	225.73	213.97	199.18	182.47	161.72
SBL	355.62	338.19	302.21	271.54	257.32	210.35
MGRD	350.55	272.28	221.94	193.28	154.37	172.96
FAD	209.18	200.68	189.76	178.14	164.54	153.85

5.4. Anchor Deployment Comparison

To demonstrate the proposed anchor-deployment strategy, we simulated 100 anchor-deployment schemes within a localization area of 900 m × 900 m. We used $SCLPercent$ and $SULPercent$ parameters to verify the efficiency of the node-deployment strategy. As shown in Fig. 13, the probability distribution of the accumulative error is markedly higher when the subarea uniformity coefficient $SULPercent > 0.5$ than that when $SULPercent < 0.5$. In particular, when $SULPercent > 0.5$ and $SCLPercent = 0.8$, the accuracy of FAD is the highest.

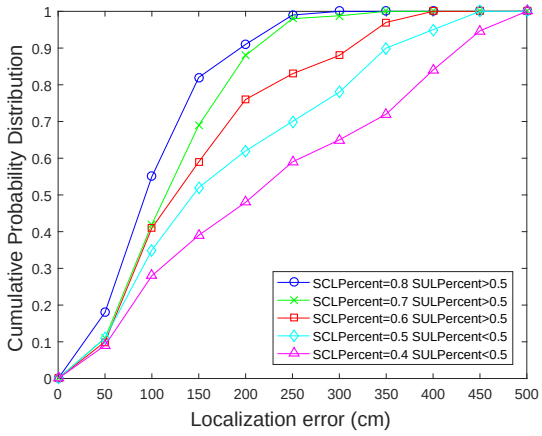

Figure 13: Localization results of different anchor deployments.

6. Real-world Shipboard Experimentation

In this section, the performance of the FAD algorithm implemented in the real-world shipboard environment was evaluated and compared with four other state-of-the-art methods. The experiment results are demonstrated.

6.1. Experiment Environment

In this study, the shipboard sensor network nodes were designed using Texas Instruments (TI) CC2530 chips, which meet the IEEE 802.15.4/ZigBee protocols and operate in the 2.4-GHz range. The sensor nodes are assigned to two roles, receiving and anchor nodes. Anchor nodes were fixed in the ship, and they continuously broadcasted radio messages at a rate of one

package per min, as shown in Fig.14. Receiving nodes were randomly placed in the hall. These nodes collect the RSSI information measured from the anchor nodes, and upload them to the server to estimate the locations. The experiment scenarios include the multipath-rich scenarios, such as a video hall and a corridor, as well as the multipath-scarce scenarios such as the main deck and the sun deck.

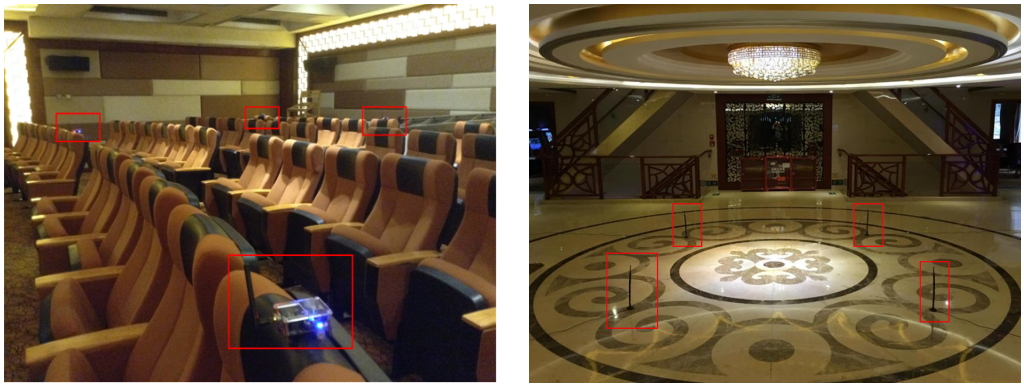

(a) Multipath-rich Scenario (b) Multipath-scarce Scenario

Figure 14: Experiment scenarios in the shipboard environment.

6.2. Experiments in Multipath-rich Scenario

The experiments in multipath-rich scenario were conducted in the video hall (15.9 m $\times$ 9.7 m) of the ship "M.S.Yangtze 2." We designed the shipboard sensor network nodes using Texas Instruments (TI) CC2530 chips, which meet the IEEE 802.15.4/ZigBee protocols and operate in the 2.4-GHz frequency band. A network of $N = 4 \ldots 9$ beacon nodes was deployed in the hall. Eighty reference locations were identified and marked by numbers on the floor, as shown in in Fig. 15. Neighboring reference locations are separated by approximately 1.5 m. The RSSI values at each location were obtained for approximately 60 samples. For comparison, we also estimated the localization of the target nodes using the five localization techniques: FAD, WCL, REWL, SBL, and MGRD. To determine the performance, we calculated the mean error and variance of these three methods. The numerical localization result is shown in Table 5. Among them, the minimum and maximum positioning errors of the FAD are 1.30 m and 2.10 m, respectively. As can be seen, the FAD outperforms the other four methods regardless of

the number of anchors. This shows that multipath propagation degrades the accuracy of the RSSI-based localization as well as shadowing in multiple room environments. Meanwhile, the FAD is sufficiently robust to overcome the degradation introduced by the multipath effect.

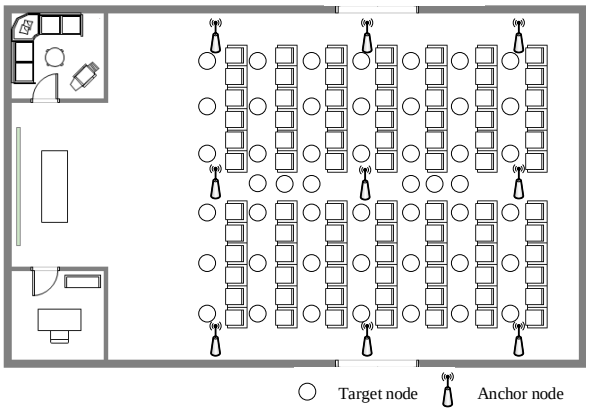

Figure 15: Video hall and locations of anchor nodes.

6.3. Experiments in Multipath-scarce Scenario

We intended to quantify the performance of the FAD in an environment representing a multipath-scarce scenario. The experiments were conducted on the main deck of "M.S.Yangtze 2" with an area of 9 m $\times$ 9 m, as shown. The networks of nine anchor nodes that were deployed on the deck can be viewed in Fig.14(b). A target node is bound to an experimenter, who walked along the pathway with a mean speed of 1 m/s, and the system measured the localization errors at different spots using five methods. The average error distances of each method are calculated in time. Fig. 16 shows the experiment results obtained as we varied N from four to nine. As can be seen, as the multipath effect decreased, the localization result shows a higher position-recognition accuracy than the corridors. When the number of anchors exceeded six in the experiments, the localization errors of the five methods are within 3 m. The accuracy of the FAD method is within 2 m when there are five anchors. In contrast, four other methods can achieve 2 m only when there are more than seven anchors. The error distance of the FAD ranges from 1.53 m to 2.10 m. This shows that even the RSSI values are affected by the course, speed, altitude, and movements of the ship during the

Table 5: Comparison of the mean error in multipath-rich scenario experiments (cm).

Methods \ Anchors	4	5	6	7	8	9
WCL	246.15	220.35	197.99	176.85	159.92	144.74
REWL	224.58	225.72	178.81	158.43	145.07	138.58
SBL	378.35	359.46	342.60	315.18	276.45	272.85
MGRB	320.27	314.24	284.32	262.07	231.51	224.16
FAD	210.48	189.45	168.36	151.08	139.72	130.23

voyage, and that FAD performs better than the four other state-of-the-art methods in shipboard environments.

Fig. 17 shows the true locations of the target nodes with the estimated locations calculated by the FAD. The figure also shows the subareas divided by the boundaries between all pairs of anchor nodes. The circles represent the actual positions of the target nodes, and the stars represent the estimated positions that are obtained by using the FAD. The lines represent the boundaries introduced by nine anchor nodes, which are represented by blocks. Among them, the average positioning error of FAD is 1.44 m.

6.4. Experiment of Environmental Changes

In this part, we investigate how environmental changes affect the FAD performance. To maximize the effect of environmental change, the corridor scenario that had the most watertight doors and passengers was chosen to conduct the evaluation. First, we obtained RSSI data from 20 reference locations with separation of 0.5 m in the corridor. After that, we changed the environment by altering all of the room doors, after which the RSSI data were again obtained. Then, we changed the environment further by introducing randomly walking persons and collecting data for the third data set. Table 6 describes these environmental changes in the data sets.

The difference in the RSSI data after the environmental change is demonstrated in Fig. 18. Among them, the above one shows the RSSI difference

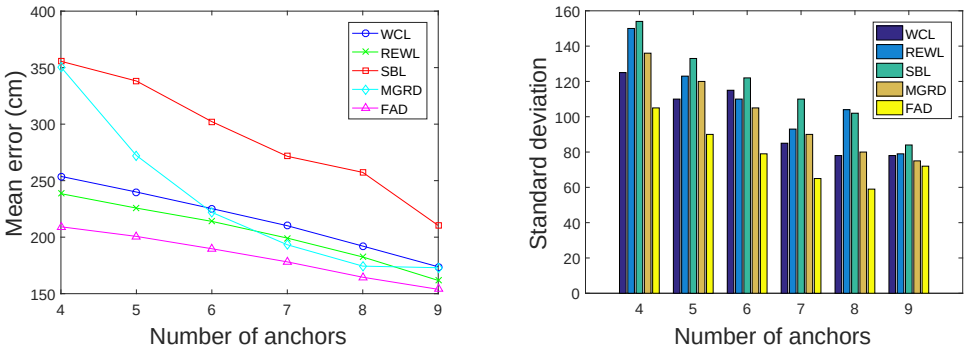

(a) Mean error (b) Standard deviation

Figure 16: Mean error and variance of the localization methods in multipath-scarce scenario.

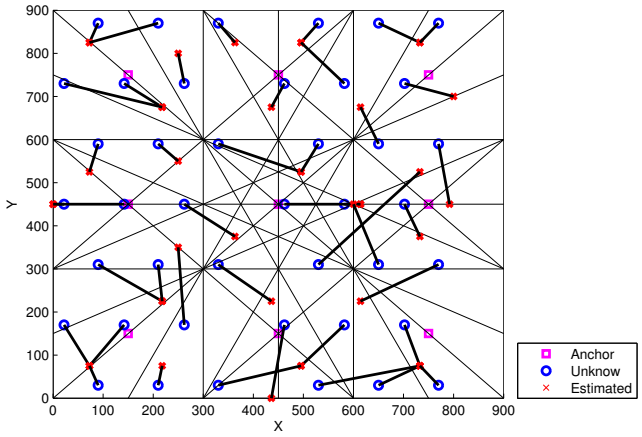

Figure 17: Comparison between true locations and FAD location estimates.

Table 6: Environment changes data sets.

Data Set	**Passengers**	**Doors**
Set 1	None	Close
Set 2	None	Open
Set 3	Exist	Open

of Set 1 and Set 2. As can be seen, the decreasing trend of the RSSI after changing the environment behaves in a similar manner or even slightly better than the environment with all doors closed. As the propagation distance increased, the RSSI value decreased constantly. This is because closing doors introduced several reflection paths and severe multipath effects because the signals bounced off the doors, thus decreasing the accuracy of the localization method. Based on this characteristic, the FAD, which uses the high–low relationship of RSSI can work even better than the formal environment. Furthermore, we evaluated the performance of the FAD with these data sets. The average accuracies of each target located in the right subarea of each data set are shown in Table 7. The results show that at first, the FAD method can achieve a good subarea-localization accuracy of 92.3%. After changing the environment by opening all of the doors, the average accuracy achieved was 96.2%.

However, the impact of the randomly walking passengers in the shipboard environment is irregular, and it is difficult to find a pattern, making object localization using RSSI a challenging task. Fig. 18 illustrates the difference in the RSSI of Set 3. As can be seen, the RSSI measurements at different distances have different variant trends. For example, the RSSI for a transmission distance of 5 m is higher than that for 6 m, but the RSSI for 8 m is lower than that for 9 m. In Table 7, we can also see that the average accuracy degrades drastically after introducing the random walking passengers. This is because the passengers would shelter the signal and significantly change the RSSI values. In this case, the FAD that utilizes the fault-torrent mechanism performs better than the SBL.

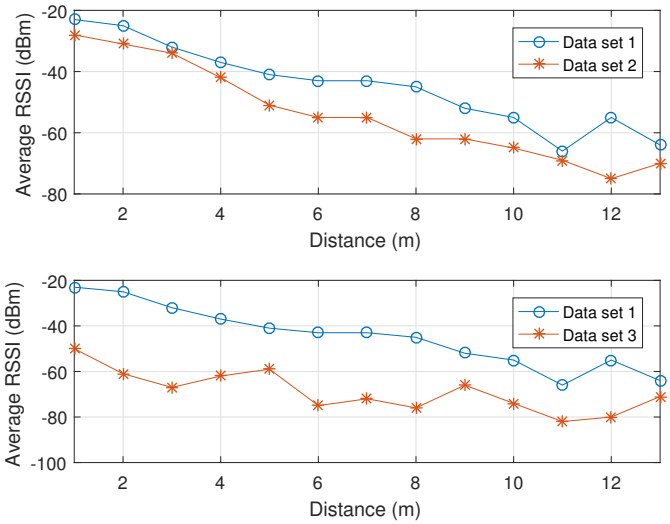

Figure 18: RSSI in testing locations in data sets.

Table 7: Subarea localization accuracy degradation caused by environment changes.

Environment changes	**Accuracy**	
	FAD	**SBL**
None	96.2%	85.0%
Opening doors	98.2%	87.5%
Random walking passengers	77.5%	53.8%

7. Related Work

Recently, there has been much work on range-free localization techniques in WSNs[27] [28] [29] [30]. Among them, two localization methods utilized the high–low relationship instead of actual RSSI values as the signature for localization. In [27], an SBL technique was proposed to identify the target node location by a unique set of anchor-node IDs. The target node determines its set of area signature sequences by measuring the RSSI and estimating its location by searching through the location sequence table with the highest similarity of matched sequence. In [28], Shang et al. proposed an RF-based localization technique called MRGD, which utilized the Voronoi diagram to divide the localization region into sub-regions, and the Lagrange multiplier method to calculate the target node location. These methods achieve low computation costs in WSNs; however, they have some drawbacks, including that the SBL will never reach the maximum number of subareas as shown by their equations in the paper, and they will also suffer the severe asymmetry problem of the RSSI measurement from anchors when performing in the shipboard environment. The drawback of MRGD is that only three nearest anchor nodes are considered to determine the subregion, which will lead to the coarse-grained location result in the sparse networks of anchor nodes. Our work deals with this problem effectively by using a fault-tolerant mechanism, and we achieved a fine-grid result.

However, the above methods ignore the practical scenario, and do not recognize that the spatial deployment of anchor nodes is important to the robustness of the localization scheme. Beyond them, there is a recent work that considers the anchor deployment in WSN-based localization applications. In [31], a heuristic approach is presented to overcome the subarea heterogeneous problem by minimizing the area standard deviation, and the effect was mathematical analyzed. However, it only considered the factor of the maximum number of partitions, which cannot represent the subarea standard deviation comprehensively. Although numerous issues need to be considered to achieve the optimal anchor deployment, three factors should first be considered: (1) the maximum number of subareas, (2) the convergence level of subareas, and (3) the uniform level of the area division result. These factors form our motivation to search for the optimal anchor deployments methods. In summary, this paper focuses on solving the interference in shipboard environments by applying a fault-torrent mechanism and employing an optimal anchor-deployment strategy in order to obtain a higher

localization accuracy.

8. Conclusion and Future Work

In this paper, we proposed a novel range-free localization method called FAD, which does not require significant computational resources, and which achieves high accuracy to meet the requirement of shipboard applications. The proposed method utilizes the high–low relationship of RSSI to estimate the location of target nodes. We also investigated the shipboard RSSI signals and proposed a fault-tolerant mechanism that enhances the robustness of the proposed method. We performed simulations and real-world experiments, and the results show that our FAD can achieve a localization error distance of 1.89 m when we deployed five anchors, 1.68 m with six anchors, 1.51 m with seven anchors, and 1.30 m with nine anchors, as well as demonstrate the desirable performance of FAD. With fewer anchor nodes and a less complicated localization algorithm, the FAD is capable of quickly determining the location of staff and cargo in cabins in an accurate and reliable manner.

In future work, we aim to incorporate the location probability into the fault-tolerant mechanism and use more advanced error models to further improve the accuracy of the FAD. The real-world experiment space is restricted by the video hall construction, and we did not test the fuzzy-boundary mechanism. To evaluate the performance of FAD systematically, we will perform additional experiments in wide shipboard spaces and with a large-scale WSN system. Furthermore, we will also investigate ways of achieving localization in 3D environments as well as locating multiple objects.

Acknowledgements

This work was supported in part by the National Natural Science Foundation of China (NSFC) under Grant No. 51279151, the Major Project for the Technology Innovation of Hubei Province, China, under Grant No.2017AAA120 and the Fundamental Research Funds for the Central Universities under Grant No. WUT-2017-YB-318.

References

[1] J. Wang, J. Lin, S. Xie, The environment monitoring system based on wireless sensor network, World Automation Congress 28 (11) (2015) 1732–1740. doi:10.3969/j.issn.1004-1699.2015.11.026.

[2] M. Ibrahim, O. Moselhi, Inertial measurement unit based indoor localization for construction applications, Automation in Construction 71 (2016) 13–20. doi:10.1016/j.autcon.2016.05.006.

[3] H. M. Khoury, V. R. Kamat, Evaluation of position tracking technologies for user localization in indoor construction environments, Automation in Construction 18 (4) (2009) 444–457. doi:10.1016/j.autcon.2008.10.011.

[4] B. Wang, S. Zhou, W. Liu, Y. Mo, Indoor Localization Based on Curve Fitting and Location Search Using Received Signal Strength, IEEE Transactions on Industrial Electronics, 62 (1) (2015) 572–582. doi:10.1109/TIE.2014.2327595.

[5] Y. Shi, Improving the performance of RSS detection using wireless open-source platforms, Texas Symposium on Wireless and Microwave Circuits and Systems 47. doi:10.1109/WMCaS.2015.7233207.

[6] H. Kdouh, C. Brousseau, G. Zaharia, G. Grunfelder, G. El-Zein, Applying ubiquitous wireless technologies for shipboard monitoring systems, 14th International Symposium on Wireless Personal Multimedia Communications 71 (2011) 1–5. doi:10.5772/32748.

[7] J. Elson, L. Girod, D. Estrin, Fine-grained network time synchronization using reference broadcasts, ACM SIGOPS Operating Systems Review 36 (SI) (2002) 147. doi:10.1145/844128.844143.

[8] S. Ganeriwal, R. Kumar, M. B. Srivastava, Timing-sync protocol for sensor networks, Proceedings of the first international conference on Embedded networked sensor systems 2 (2003) 138. doi:10.1145/958507.958508.

[9] T. He, C. Huang, B. M. Blum, J. A. Stankovic, T. Abdelzaher, Range-free localization schemes for large scale sensor networks, Proceedings of the 9th annual international conference on Mobile computing and networking 2 (2003) 81. doi:10.1145/938994.938995.

[10] H. Kdouh, C. Brousseau, G. Zaharia, G. Grunfelder, G. E. Zein, A realistic testing of a shipboard wireless sensor network, Military Technical Academy Review 2 (2013) (2013) 107–120. doi:10.1843.3391.

[11] P. Pivato, L. Palopoli, D. Petri, Accuracy of RSS-based centroid localization algorithms in an indoor environment, IEEE Transactions on Instrumentation and Measurement 60 (10) (2011) 3451–3460. doi:10.1109/TIM.2011.2134890.

[12] P. Sommer, R. Wattenhofer, Gradient clock synchronization in wireless sensor networks, Proceedings of the 2009 International Conference on Information Processing in Sensor Networks (2009) 37–48doi:10.5353/b5204913.

[13] G. Tong, C. Liu, Supporting Soft Real-Time Sporadic Task Systems on Uniform Heterogeneous Multiprocessors with No Utilization Loss, IEEE Transactions on Parallel and Distributed Systems 27 (9) (2016) 2740–2752. doi:10.1109/TPDS.2015.2503278.

[14] S. Nawaz, N. Trigoni, Convex programming based robust localization in NLOS prone cluttered environments, 10th International Conference on Information Processing in Sensor Networks 2 (2011) 318–329. doi:10.1109/wcnc.2016.7564801.

[15] Q. Zhang, Z. Zhou, W. Xu, J. Qi, C. Guo, P. Yi, T. Zhu, S. Xiao, Fingerprint-free tracking with dynamic enhanced field division, IEEE Conference on Computer Communications 26 (2015) 2785–2793. doi:10.1109/INFOCOM.2015.7218671.

[16] M. Brunato, R. Battiti, Statistical learning theory for location fingerprinting in wireless LANs, Computer Networks 47 (6) (2005) 825–845. doi:10.1016/j.comnet.2004.09.004.

[17] S.-H. Fang, C.-H. Wang, A Novel Fused Positioning Feature for Handling Heterogeneous Hardware Problem, IEEE Transactions on Communications 63 (7) (2015) 2713–2723. doi:10.1109/TCOMM.2015.2442989.

[18] Y. Shang, W. Ruml, Y. Zhang, M. P. J. Fromherz, Localization from mere connectivity, ACM International Symposium on Mobile ad hoc networking & computing (2003) 201.doi:10.1145/778435.778439.

[19] D. Niculescu, B. Nath, DV based positioning in ad-hoc networks, Springer Journal on Telecommunication Systems 22 (1) (2003) 267–280. doi:10.1023/A:1023403323460.

[20] Z. Zhong, Achieving Range-free Localization Beyond Connectivity, Proceedings of the 7th ACM Conference on Embedded Networked Sensor Systems (2009) 281–294.doi:10.1145/1644038.1644066.

[21] P. Chen, Z. Zhong, T. He, Bubble trace: Mobile target tracking under insufficient anchor coverage, Proceedings - International Conference on Distributed Computing Systems (2011) 770–779.doi:10.1109/ICDCS.2011.56.

[22] K. Chintalapudi, A. Padmanabha Iyer, V. N. Padmanabhan, Indoor localization without the pain, 16th Annual International Conference on Mobile Computing and Networking (2010) 318–329.doi:10.1145/1859995.1860016.

[23] A. Arya, P. Godlewski, M. Campedel, G. Du Chene, Radio database compression for accurate energy-efficient localization in fingerprinting systems, IEEE Transactions on Knowledge and Data Engineering 25 (6) (2013) 1368–1379. doi:10.1109/TKDE.2011.241.

[24] M. Liu, H. Leung, A. Maddumabandara, Experimental Evaluation of Indoor Localization Using Wireless Sensor Networks, IEEE Sensors Journal PP (99) (2015) 1–1. doi:10.1109/JSEN.2015.2438193.

[25] K. Liu, T. Yang, J. Ma, Z. Cheng, Fault-Tolerant Event Detection in Wireless Sensor Networks using Evidence Theory, KSII Transaction on Internet and Infomation Systems 9 (10) (2015) 3965–3982. doi:10.3837/tiis.2015.10.011.

[26] B. Sklar, Rayleigh fading channels in mobile digital communication systems Part I: Characterization, IEEE Communications Magazine 35 (9) (1997) 136–146. doi:10.1109/35.620535.

[27] K. Yedavalli, B. Krishnamachari, Sequence-Based Localization, IEEE Transactions on Mobile Computing 7 (1) (2008) 1–14. doi:10.1109/TMC.2008.4387797.

[28] F. Shang, Y. Jiang, A. Xiong, W. Su, L. He, A Node Localization Algorithm Based on Multi-Granularity Regional Division and the Lagrange Multiplier Method in Wireless Sensor Networks, Sensors 16 (11) (2016) 1934. doi:10.3390/s16111934.

[29] H. Li, G. Chan, J. K. W. Wong, M. Skitmore, Real-time locating systems applications in construction, Automation in Construction 63 (2016) 37–47. doi:10.1016/j.autcon.2015.12.001.

[30] Glover, Unsupervised Indoor Localization, Duke University 127 (1389) (2014) 17–25. doi:10.1145/2307636.2307655.

[31] Q. Zhang, W. Xu, Z. Huang, Z. Zhou, P. Yi, T. Zhu, S. Xiao, Context-centric target localization with optimal anchor deployments, Proceedings of International Conference on Network Protocols (2016) 396–405doi:10.1109/ICNP.2015.14.